Journal of Magnetic Resonance **140,** 351–362 (1999)
Article ID jmre.1999.1834, available online at http://www.idealibrary.com on IDEAL®

Sodium Ions in Ordered Environments in Biological Systems: Analysis of ^{23}Na NMR Spectra

Richard Kemp-Harper, Bill Wickstead,[1] and Stephen Wimperis

Physical Chemistry Laboratory, University of Oxford, South Parks Road, Oxford OX1 3QZ, United Kingdom

Received October 21, 1998

Experiments that selectively excite $I = \frac{3}{2}$ nuclei exhibiting residual quadrupolar splittings are used to acquire ^{23}Na NMR spectra from a range of biologically relevant samples containing sodium in ordered environments. Three complementary approaches to the analysis of such spectra are described: (i) measurement of relaxation rates, (ii) extraction of homogeneous linewidths from two-dimensional Jeener–Broekaert spectra, and (iii) simultaneous fitting of detailed theoretical functions to a series of one-dimensional Jeener–Broekaert spectra. Analysis of relaxation rates provides evidence for compartmentation in bovine nasal cartilage. Each approach is used to demonstrate the presence of anisotropy in transverse relaxation in porcine tendon. For certain samples containing collagen, a good theoretical fit to the spectra was obtained using a model that allows for anisotropic relaxation by including the effects of slow lateral and radial diffusion.

INTRODUCTION

The NMR behavior of spin $I = \frac{3}{2}$ nuclei in biological systems is dominated by the quadrupolar interaction. This interaction of the nuclear quadrupole moment with the local electric field gradient is responsible for the appearance of splittings in the NMR spectrum and is the dominant mechanism for relaxation. Recent NMR studies of spin $I = \frac{3}{2}$ nuclei in biological systems have demonstrated the presence of spins exhibiting residual quadrupolar splittings (*1–4*). Such spectra have been observed using ^{23}Na and ^{35}Cl NMR and in samples ranging from cell suspensions to excised tissues and even human tissues *in vivo* (*1–10*). The residual splittings have been shown to arise from the association of the ions with ordered structures such as collagen or cell membranes (*2, 4, 9, 11*). A number of experiments have been developed that allow selective excitation of this pool of "ordered" ions by selection of particular coherence pathways (*1, 3, 6, 12–15*). Detailed, quantitative analysis of the spectra is imperative if the nature of the ionic environment and the interactions responsible for the experimental observations are to be elucidated. A number of studies have included analysis of the resulting spectra and have shown that quantitative information may be obtained (*4, 9, 16*).

[1] Present address: School of Biological Sciences, University of Manchester, Oxford Road, Manchester M13 9PT, United Kingdom.

The purpose of the current work is to demonstrate the use of three complementary analysis techniques that allow the detailed study of ions in ordered environments and to apply these methods to the investigation of the environment of sodium in a number of systems.

It is convenient to express the time evolution of the density operator for spin $I = \frac{3}{2}$ nuclei in the irreducible spherical tensor operator basis and examples of this application can be found in Refs. (*1, 3, 17*). Expressions for the time evolution of transverse single-quantum coherence resulting from quadrupolar splitting and pure biexponential relaxation have been given in Ref. (*3*). From these expressions and other analyses, it becomes clear that, while both quadrupolar splitting and biexponential relaxation contribute to the formation of odd-rank tensors $T_{1,\pm1}$ and $T_{3,\pm1}$, only the presence of residual quadrupolar splitting allows the formation of second-rank tensors $T_{2,\pm1}$. Thus the key to selective excitation of ordered spins is the selection of solely this component of the density operator.

A modified version of the Jeener–Broekaert experiment (*3, 18*) and a modified double-quantum filtration experiment (*1, 17*) have been used to achieve selective excitation of ordered ^{23}Na spectra. The pulse sequences for these two experiments are shown in Figs. 1a and 1b, respectively. The Jeener–Broekaert experiment performs the selection by exciting a state of quadrupolar order, $T_{2,0}$, which can only be created if second-rank tensors are present. The double-quantum filtration experiment selects the contribution of second-rank tensors by virtue of a flip-angle effect that suppresses unwanted third-rank double-quantum coherence. The efficiency and properties of these two experiments have been compared elsewhere (*3, 14*).

The spectra obtained using either of these experiments correspond to the tensor $T_{2,-1}$ and are characteristic antiphase powder patterns containing intensity *only* in the "satellite" transitions ($|m_I = \frac{3}{2}\rangle$ to $|m_I = \frac{1}{2}\rangle$ and $|m_I = -\frac{1}{2}\rangle$ to $|m_I = -\frac{3}{2}\rangle$). Other experiments have been developed that select the contribution from the second-rank tensors and then return the signal intensity to the central transition ($|m_I = \frac{1}{2}\rangle$ to $|m_I = -\frac{1}{2}\rangle$) (*12*). Pulse sequences for two of these so-called "central transition recovery" (CTR) experiments are given in Figs. 1c and 1d. These experiments show a gain in sensitivity with

1090-7807/99 $30.00

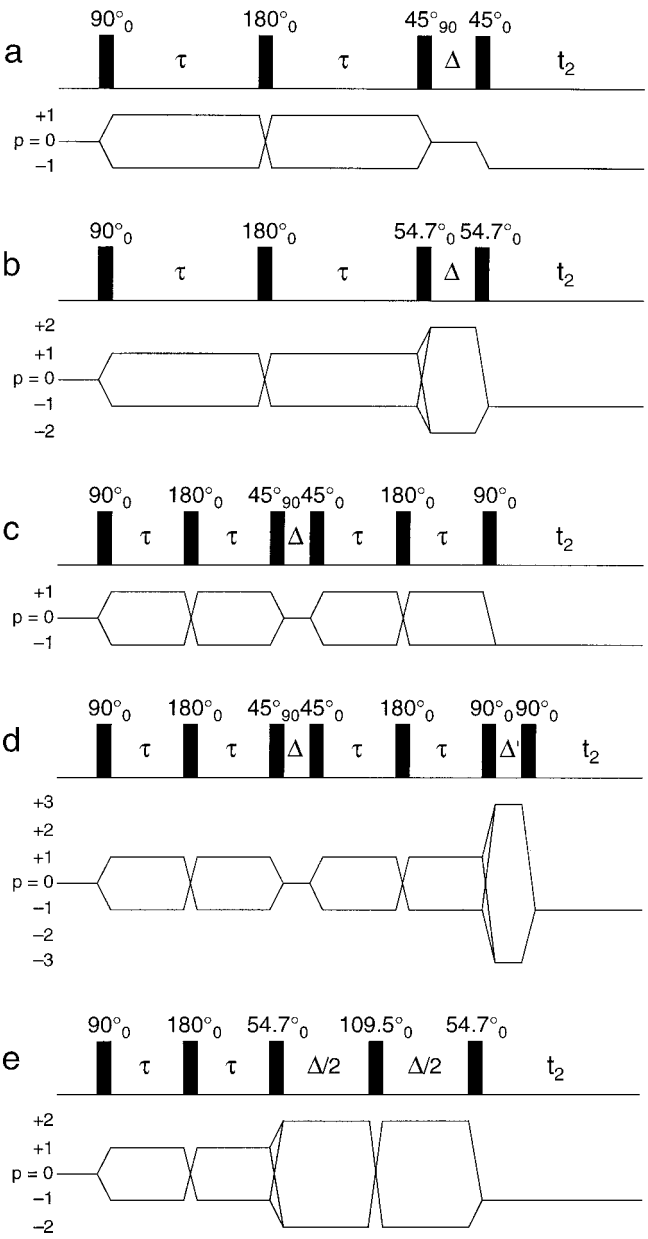

FIG. 1. Pulse sequences and coherence transfer pathway diagrams for experiments used in selective excitation of ordered sodium. (a) Jeener–Broekaert experiment. (b) Double-quantum filtration experiment. (c) Central transition recovery experiment (CTR). (d) Triple-quantum filtered central transition recovery experiment (TQF-CTR). (e) Double-quantum quadrupolar echo experiment (DQQE).

respect to the Jeener–Broekaert experiment owing to the greater sharpness of the central transition.

APPROACHES TO SPECTRAL ANALYSIS

Measurement of Relaxation Rates

The first approach to the analysis of ordered sodium spectra is the simple measurement of relaxation rates by fitting of exponential functions to a series of decay spectra. This method requires little *a priori* knowledge of the system under investigation. However, care must be taken that (a) only signal from ordered ions contributes to the spectra and (b) the observed decay is expected to be purely a function of relaxation and not splitting. Objective (a) can be achieved using the experiments introduced above which selectively excite ordered sodium. Objective (b) is achieved if either the time evolution of the spin $I = \frac{3}{2}$ density operator is independent of splitting or a quadrupolar echo can be formed, thus refocusing any quadrupolar splitting evolution. States of the density operator for which these objectives may be achieved and relaxation rates measured include quadrupolar order, triple-quantum coherence, and second-rank double-quantum coherence.

Quadrupolar relaxation through modulation of the quadrupolar interaction is assumed to be the only mechanism throughout. The contributions to relaxation of dipolar interactions (*19*) and modulation of the local director (*20*) have been neglected. The calculation of relaxation rates from the relevant Redfield matrices can be found in Ref. (*17*) for the case where all transitions are degenerate. When quadrupolar splittings are dominant this degeneracy is lifted, the cross-relaxation terms can be neglected, and the calculation becomes trivial. The relaxation rates $R_i^{(p)}$, where p is the coherence order and the label i follows the convention of Ref. (*17*), can be expressed as

$$R_2^{(0)} = 2K\{J_1(\omega_0) + J_2(2\omega_0)\} \quad [1a]$$

$$R_1^{(1)} = K\{J_0(0) + J_1(\omega_0) + J_2(2\omega_0)\} \quad [1b]$$

$$R_2^{(1)} = K\{J_1(\omega_0) + J_2(2\omega_0)\} \quad [1c]$$

$$R^{(2)} = K\{J_0(0) + J_1(\omega_0) + J_2(2\omega_0)\} \quad [1d]$$

$$R^{(3)} = K\{J_1(\omega_0) + J_2(2\omega_0)\}, \quad [1e]$$

where $K = (\frac{1}{40})\,(e^2qQ/\hbar)^2\,(1 + \eta^2/3)$ and $J_0(0)$, $J_1(\omega_0)$, and $J_2(2\omega_0)$ are the spectral densities describing the motion responsible for the relaxation.

Quadrupolar order, $T_{2,0}$, is a population state that is not affected by quadrupolar splitting or resonance offset and, for spin $I = \frac{3}{2}$, relaxes exponentially (*3, 17*). The Jeener–Broekaert experiment (Fig. 1a) and the two central transition recovery experiments (Figs. 1c and 1d) can be adapted to measure relaxation of $T_{2,0}$ by simply incrementing the interval Δ to yield a series of spectra to which a decaying exponential function can be fitted. The main advantage of the CTR experiments in this application is that, while the Jeener–Broekaert experiment yields spectra with intensity only in the satellites, they return intensity to the sharp central transition. This results in a gain in sensitivity and an increase in the ease of "peak picking," making these experiments particularly suitable for the measurement of relaxation.

The TQF-CTR experiment in Fig. 1d can also be adapted to measure the relaxation of triple-quantum coherence, $T_{3,\pm 3}$. Although this can be achieved using a conventional triple-quantum filtration experiment, the TQF-CTR experiment first excites quadrupolar order, ensuring that the relaxation rate measured is that of ordered spins alone with no contribution from spins in an isotropic slow-motion regime. The adaptation of the TQF-CTR experiment for the measurement of triple-quantum relaxation is exactly analogous to that described in Ref. (*21*) for the conventional triple-quantum filtration experiment and involves insertion of an additional 180° refocusing pulse into the middle of the Δ' interval and incrementation of this interval. Triple-quantum coherence evolution is independent of quadrupolar splitting so a simple exponential function can be fitted to the decay spectra.

It is worth noting from Eq. [1] that $R_2^{(0)} = 2R^{(3)} = 2R_2^{(1)}$. Thus measurement of the relaxation rates $R_2^{(0)}$ and $R^{(3)}$ provides an estimate of the transverse relaxation rate of the central transition of the powder pattern. Further examination of Eq. [1] reveals that $R^{(2)} = R_1^{(1)}$, so measurement of the relaxation rate of in-phase double-quantum coherence gives an estimate of the transverse relaxation rate of the satellites in the powder pattern spectrum. It might be expected that $R^{(2)}$ could be measured using the double-quantum filtration experiment in Fig. 1b by analogy with the triple-quantum relaxation experiment. Unfortunately, the time evolution of double-quantum coherence is dependent on quadrupolar splitting. However, as described in Ref. (*13*), it is possible to form a complete quadrupolar echo for double-quantum coherence by employing a pulse with a flip angle of 109.5° as the refocusing pulse in the center of the evolution period. This double-quantum quadrupolar-echo (DQQE) experiment, shown in Fig. 1e, allows, via incrementation of the interval Δ, the measurement of double-quantum coherence relaxation independently of the quadrupolar splitting.

Extraction of Linewidths from Two-Dimensional Jeener–Broekaert Spectra

The direct measurement of the relaxation rate of single-quantum coherence is not possible because the time evolution of single-quantum coherences is dependent on quadrupolar splitting and a perfect quadrupolar echo cannot be formed for $I = \frac{3}{2}$. However, one approach to the analysis of ordered sodium spectra uses the favorable properties of two-dimensional lineshapes to extract the homogeneous linewidth of the satellite transitions, and hence their transverse relaxation rate, by fitting to cross sections through a two-dimensional spectrum.

A two-dimensional Jeener–Broekaert experiment has been described in Ref. (*16*). In this experiment, the $t_1 = 2\tau$ period in Fig. 1a is incremented, yielding a two-dimensional data set in which the evolution in t_1 is the same as that in t_2. The two-dimensional spectrum therefore consists of two ridges along opposing diagonals $F_1 = F_2$ and $F_1 = -F_2$, assuming the transmitter frequency is on-resonance. The Jeener–Broekaert experiment is inherently amplitude-modulated and it is therefore possible to obtain pure absorption lineshapes in F_1. However, the necessity in the experiment for a 90° phase difference between the initial pulse and the first 45° pulse means that it is not possible to obtain a cosine-modulated signal in addition to the sine-modulated signal, and hence sign discrimination in F_1 cannot be achieved. The spectrum is therefore obtained by using a real Fourier transform in F_1 and only positive frequencies are displayed.

The ridges in the spectra are the result of the presence of the inhomogeneous quadrupolar broadening in both dimensions. Brown and Wimperis (*22*) have shown that it is possible to extract the homogeneous linewidth from two-dimensional spectra in which the inhomogeneous broadening remains in both dimensions. This approach uses the favorable characteristics of two-dimensional lineshapes to extract the transverse relaxation rate by fitting an analytical function to cross sections through two-dimensional spectra. Crucially, the results obtained are insensitive to the precise form of the function used to describe the distribution of quadrupolar splittings (*16*). It has been demonstrated that homogeneous linewidths can be reliably extracted from spectra exhibiting a Gaussian distribution of splittings using a simple model lineshape based on a quadratic distribution function (*16*). Relaxation rates can therefore be extracted without a detailed model of the system. When this approach is applied to the analysis of two-dimensional Jeener–Broekaert spectra, the inhomogeneous broadening is the quadrupolar broadening of the satellite transitions and the homogeneous linewidth (full width at half height) obtained, $\Delta\nu_{1/2}$, is therefore related to the relaxation rate $R_1^{(1)}$ by the expression $R_1^{(1)} = \pi\Delta\nu_{1/2}$.

Simultaneous Fitting to One-Dimensional Jeener–Broekaert Spectra

A third approach to the analysis of ordered sodium spectra, adopted by Eliav and Navon in a previous study (*4*), involves the simultaneous fitting of a detailed theoretical model function to a series of one-dimensional spectra. The approach described here is formally identical to that employed by Eliav and Navon using double-quantum filtered methods. The Jeener–Broekaert and double-quantum filtered experiments produce essentially identical spectra and the same physical models are applied in the analysis.

In order to describe the full spin $I = \frac{3}{2}$ lineshape, it is necessary to consider the combined effect of relaxation and quadrupolar splitting. In the Zeeman Hamiltonian eigenbasis the evolution of $p = -1$ coherences can be expressed as

$$\frac{d}{dt}\boldsymbol{\sigma}^{(-1)}(t) = (-i\mathbf{H}^{(-1)} - \mathbf{R}^{(-1)})\boldsymbol{\sigma}^{(-1)}(t), \qquad [2]$$

where $\mathbf{H}^{(-1)}$ is the time-independent Hamiltonian superopera-

tor, $\mathbf{R}^{(-1)}$ is the relaxation superoperator, and $\boldsymbol{\sigma}^{(-1)}(t)$ is a vector containing the $p = -1$ elements of the density matrix,

$$\boldsymbol{\sigma}^{(-1)}(t) = \begin{pmatrix} \sigma_{21}(t) \\ \sigma_{32}(t) \\ \sigma_{43}(t) \end{pmatrix}. \quad [3]$$

The residual quadrupolar splittings observed for ^{23}Na nuclei in biological systems are of the order 0–15 kHz. Since these are relatively small, first-order perturbation theory can be used. In this limit $\mathbf{H}^{(-1)}$ is given by

$$\mathbf{H}^{(-1)} = \begin{pmatrix} -2\omega_Q & 0 & 0 \\ 0 & 0 & 0 \\ 0 & 0 & +2\omega_Q \end{pmatrix}, \quad [4]$$

where ω_Q is the residual quadrupolar splitting parameter. Ignoring the contribution from the dynamic shift, the relaxation matrix for $p = \pm 1$ coherences is given by

$$\mathbf{R}^{(\pm 1)} = \begin{pmatrix} A & 0 & B \\ 0 & C & 0 \\ B & 0 & A \end{pmatrix}, \quad [5]$$

where the elements A, B, and C are (*17*)

$$A = R_1^{(1)} = K\{J_0(0) + J_1(\omega_0) + J_2(2\omega_0)\} \quad [6a]$$

$$B = -KJ_2(2\omega_0) \quad [6b]$$

$$C = R_2^{(1)} = K\{J_1(\omega_0) + J_2(2\omega_0)\}. \quad [6c]$$

The solution to Eq. [2] has the form

$$\boldsymbol{\sigma}^{(-1)}(t) = \exp\{(-i\mathbf{H}^{(-1)} - \mathbf{R}^{(-1)})t\}\ \boldsymbol{\sigma}^{(-1)}(0). \quad [7]$$

Time-domain evolution functions for tensor operators, $\lambda_{l'l}^{(-1)}(t)$, can be derived by evaluation of the matrix $\exp\{(-i\mathbf{H}^{(-1)} - \mathbf{R}^{(-1)})t\}$ followed by transformation into the tensor basis. Dinesen and Sanctuary have presented this time-domain calculation (*23*).

The time-domain signal observed in NMR of spin $I = \frac{3}{2}$ nuclei is the result of the evolution of $T_{l,-1}$ into $T_{1,-1}$ during the acquisition period. The function $\lambda_{1l}^{(-1)}(t)$, therefore, describes the FID characteristic of the tensor $T_{l,-1}$. A Fourier transform of this function, $\Lambda_{1l}^{(-1)}(\omega)$, will thus give the spectral lineshape. It is possible to calculate the frequency-domain lineshapes without first calculating the time-domain functions by means of a Fourier–Laplace transform (*24*). This states that the Fourier transform of any function of the form

$$\mathbf{f}(t) = \exp\{\mathbf{A}t\}, \quad [8]$$

where $\mathbf{A}$ is an evolution operator or superoperator, is given by

$$\mathbf{F}(\omega) = [\mathbf{A} - i\omega\mathbf{E}]^{-1}, \quad [9]$$

where $\mathbf{E}$ is the unit operator in the same space as $\mathbf{A}$. The matrix $\boldsymbol{\Lambda}^{(-1)}(\omega)$ is thus given, in the tensor operator basis, by the expression

$$\boldsymbol{\Lambda}^{(-1)}(\omega) = [\mathbf{U}^{(-1)}\{-i\mathbf{H}^{(-1)} - \mathbf{R}^{(-1)}\}\{\mathbf{U}^{(-1)}\}^{-1} - i\omega\mathbf{E}]^{-1}, \quad [10]$$

where $\mathbf{U}^{(-1)}$ is the unitary transformation operator which transforms the Zeeman eigenbasis into the tensor operator basis, given by

$$\mathbf{U}^{(-1)} = \begin{pmatrix} \sqrt{\frac{3}{10}} & \sqrt{\frac{2}{5}} & \sqrt{\frac{3}{10}} \\ \sqrt{\frac{1}{2}} & 0 & -\sqrt{\frac{1}{2}} \\ \sqrt{\frac{1}{5}} & -\sqrt{\frac{3}{5}} & \sqrt{\frac{1}{5}} \end{pmatrix}. \quad [11]$$

Substituting the expressions for $\mathbf{U}^{(-1)}$, $\mathbf{H}^{(-1)}$, and $\mathbf{R}^{(-1)}$ into Eq. [10] gives an analytical expression for $\boldsymbol{\Lambda}^{(-1)}(\omega)$. The Jeener–Broekaert lineshape is a result of only one element, which can be written

$$\Lambda_{12}^{(-1)}(\omega) = -i\,\frac{\sqrt{3}}{\sqrt{5}}\,\frac{2\omega_Q}{\{(A + i\omega)^2 + 4\omega_Q^2 - B^2\}}. \quad [12]$$

In this work, a simultaneous fit to a series of Jeener–Broekaert spectra recorded with different values of the evolution time 2τ is performed and it is necessary to also calculate the expected amplitude of each spectrum. The amplitude of the spectrum will depend upon the amount of second-rank tensor produced during the evolution time. Hence, to simulate spectra from such an experiment the lineshape function, $\Lambda_{12}^{(-1)}(\omega)$, must be multiplied by the time-evolution function, $\lambda_{21}^{(-1)}(2\tau)$. The full expression for the lineshape is therefore

$$\lambda_{21}^{(-1)}(2\tau)\Lambda_{12}^{(-1)}(\omega) = \frac{12}{5}\,\frac{\omega_Q^2 \exp\{-2A\tau\}\,\sin\{2\sqrt{(4\omega_Q^2 - B^2)}\,\tau\}}{\{(A + i\omega)^2 + 4\omega_Q^2 - B^2\}\,\sqrt{(4\omega_Q^2 - B^2)}}, \quad [13]$$

where A and B are the relaxation matrix elements given by Eqs. [6a] and [6b], respectively.

This expression is a function of the quadrupolar splitting, ω_Q, and the spectral densities. These fundamental parameters are dependent on the local environment of the ions. Fitting of this function to experimental data using different theoretical

models allows detailed study of the motion and environment of sodium in ordered biological systems. Five such theoretical models, previously introduced by Eliav and Navon, are examined here.

Motional Models

The residual quadrupolar splitting parameter ω_Q can be expressed as

$$\omega_Q = \tfrac{1}{2}\,\omega_Q^{max}\,(3\cos^2\theta - 1), \qquad [14]$$

where θ is the angle between the magnetic field and the local director (*4*). The quadrupolar interaction is also responsible for relaxation, and the efficiency of relaxation is described in terms of the spectral densities, as in Eq. [1]. For isotropic motion, where the correlation time τ_c is single-valued, the spectral density functions take the simple form

$$J_n(\omega) = J(\omega) = \frac{2\tau_c}{1 + \omega^2\tau_c^2}. \qquad [15]$$

However, it is likely that in heterogeneous biological systems, particularly in the presence of quadrupolar splittings, the spectral density functions will take a more complex form.

The simplest model of a system which might be considered is one in which ω_Q is single-valued (i.e., there exists a unique ^{23}Na environment and macroscopic order). For biological samples this is clearly unrealistic and is not used in the fits. The next level of complexity is to allow macroscopic disorder of a single ^{23}Na environment. Model A will be defined here as one in which θ is distributed randomly, but ω_Q^{max} and also τ_c are single-valued. This model can only apply in samples which are homogeneous with well-defined anisotropic binding sites for sodium ions. The Jeener–Broekaert spectrum will take the form of a well-defined antiphase Pake powder pattern. The fits of data to Model A include three independent variable parameters: the reduced variable K/ω_0, ω_Q^{max}, and $\omega_0\tau_c$.

Many biological systems are highly heterogeneous, possessing a range of environments. In such systems, the observed values of the spectral densities are an average from several types of environment and a single value of τ_c cannot be defined. Model B considers the $J_n(\omega)$ values as independent parameters based on sample heterogeneity (note that ω_Q^{max} is still single-valued). In this case, the constant K can no longer be isolated from the spectral densities and the functions $J_0(\omega)$ and $J_1(\omega)$ never appear separately. Model B thus has three independent variable parameters: ω_Q^{max}, $K\{J_0(0) + J_1(\omega_0)\}$, and $KJ_2(2\omega_0)$.

In some samples, particularly those containing oriented fibers, it is possible that tumbling motions responsible for relaxation may be affected by the anisotropy of the environment, conferring a θ-dependence to the spectral densities. Halle (*25*) presents an advanced theory of spin relaxation at cylindrical interfaces based on the Smoluchowski diffusion equation and the continuous diffusion model which will not be elucidated here. The model assumes a fast local motion combined with a much slower radial and lateral diffusion (i.e., around or perpendicular to the fibers, respectively). The long-range order case described by Halle is the case for which a residual quadrupolar coupling is observable. Assuming that the value of θ is not changing on the NMR timescale, the spectral densities are given by

$$J_n(\omega) = J_n^f(\omega) + \frac{1}{2}\sum_{m=0,2}(2 - \delta_{n,0}) \times \{[d^2_{n,m}(\theta)]^2 + [d^2_{n,-m}(\theta)]^2\}J_m^s(\omega), \qquad [16]$$

where $J_n^f(\omega)$ represents the component of the spectral density $J_n(\omega)$ arising from the fast motion and $J_m^s(\omega)$ ($m = 0, 2$) the component arising from the slow radial and lateral diffusion. The function $J_n^f(\omega)$ is assumed to be well-approximated by the isotropic form of the spectral densities (Eq. [15]) in the extreme-narrowing limit (i.e., $J_0^f(0) \approx J_1^f(\omega_0) \approx J_2^f(2\omega_0)$), while $J_m^s(\omega_0)$ and $J_m^s(2\omega_0)$ are discarded since the intensity of slow motion at the frequencies ω_0 and $2\omega_0$ is assumed to be negligible. Hence, the spectral densities are given as

$$J_1(\omega_0) = J_2(2\omega_0) = J^f \qquad [17a]$$

$$J_0(0) = J^f + \frac{1}{16}(3\cos 2\theta + 1)^2 J_0^s(0) + \frac{3}{32}(1 - \cos 2\theta)^2 J_2^s(0). \qquad [17b]$$

This model, Model C, has four independent variable parameters: ω_Q^{max}, the fast component of the spectral densities KJ^f, and the two slow components $KJ_0^s(0)$ and $KJ_2^s(0)$.

Models A to C assume that the quadrupolar coupling constant, ω_Q^{max}, is single-valued. Given the heterogeneity of biological samples already mentioned this assumption seems unrealistic. Heterogeneity of quadrupolar coupling can be introduced by having a distribution of ω_Q^{max} values. Models D and E add a Gaussian distribution of ω_Q^{max} to the motional Models B and C, respectively:

$$W(\omega_Q^{max}) = \exp\left\{-\frac{(\omega_Q^{max} - \langle\omega_Q^{max}\rangle)^2}{\Delta\omega_Q^{max}}\right\} \qquad [18a]$$

$$\langle\omega_Q^{max}\rangle - 2\Delta\omega_Q^{max} \le \omega_Q^{max} \le \langle\omega_Q^{max}\rangle + 2\Delta\omega_Q^{max}, \qquad [18b]$$

where $\langle\omega_Q^{max}\rangle$ is the mean value of ω_Q^{max} and $\Delta\omega_Q^{max}$ is a factor representing the width of the Gaussian and is considered one of the variables in the fitting routine. The independent variable parameters for Model D are $\langle\omega_Q^{max}\rangle$, $K\{J_0(0) + J_1(\omega_0)\}$,

TABLE 1
Quadrupolar Order Relaxation Rate, $R_2^{(0)}$, Measured in Bovine Nasal Cartilage Using ^{23}Na NMR

	Exponential fit		Biexponential fit			
Experiment	$R_2^{(0)}/s^{-1}$	F	$R_2^{(0)}(i)/s^{-1}$	$R_2^{(0)}(ii)/s^{-1}$	Ratio i:ii	F
Jeener–Broekaert	106	0.024	93.0	850	1.0:0.17	0.004
CTR	101	0.025	89.5	960	1.0:0.19	0.006
TQF-CTR	97.5	0.022	86.5	780	1.0:0.18	0.004

$KJ_2(2\omega_0)$, and $\Delta\omega_Q^{max}$. Those for Model E are $\langle\omega_Q^{max}\rangle$, KJ^f, $KJ_0^s(0)$, $KJ_2^s(0)$, and $\Delta\omega_Q^{max}$.

Note that, although some samples exhibit a degree of macroscopic ordering, i.e., have a nonspherical distribution of θ, this possibility has not been included in the fits. These spectra also exhibit heterogeneity and since a Gaussian distribution of quadrupolar splittings accounts adequately for the spectra, the addition of extra parameters has not been found to be warranted.

RESULTS

Relaxation Rates

Relaxation rates were measured for two samples: bovine nasal cartilage and porcine Achilles tendon. Experiments were carried out at 79.5 MHz on a Bruker Biospec spectrometer using a custom-built, 20-mm-diameter solenoidal coil that yields both high sensitivity and a homogeneous B_1 field with a 180° pulse length of 70 μs. The porcine tendon sample displays macroscopic ordering with fibers running along the length of the tendon. For this reason two sets of measurements were made with the tendon oriented parallel and perpendicular to the static magnetic field. Bovine nasal cartilage does not exhibit any macroscopic ordering, and there is no effect on the spectra of orientation with respect to the magnetic field.

For the Jeener–Broekaert experiment on the bovine nasal cartilage sample, 128 transients were accumulated per increment while the CTR experiments required 192 to complete the phase cycle. Owing to the large volume of sample, the signal-to-noise ratio was high and no weighting was applied to the time-domain data prior to Fourier transformation. The results of fitting exponential functions to the experimental data are shown in Table 1. The value of F given in this and other tables is the normalized final root-mean-square difference between the theoretical function and the experimental data. Three quadrupolar order relaxation rates, $R_2^{(0)}$, as measured using the three different experimental methods, are shown. However, fitting a biexponential function results in a statistically significant improvement to the fit and two rates, one approximately an order of magnitude faster than the other. The results of these biexponential fits are also summarized in Table 1. This deviation from monoexponential relaxation may be attributable to compartmentation of the sample, with only slow exchange between the compartments. Further work is necessary to confirm the presence of multiexponential relaxation in these systems. Nevertheless, this observation demonstrates the utility of the measurement of the relaxation rate $R_2^{(0)}$ in biological systems.

The triple-quantum relaxation rate, $R^{(3)}$, was measured to be 41.4 s^{-1} using the TQF-CTR experiment. No line-broadening was applied. Values for the triple-quantum relaxation are expected, from Eq. [1], to be half of that measured for quadrupolar order. There is good agreement with the slow components derived from the biexponential fits. There was no significant improvement in the fit by applying a biexponential function to the triple-quantum relaxation data. It is likely that the fast component is lost during the refocusing pulse required in this experiment, 70 μs in this case.

Results obtained using the DQQE experiment (creation time, $2\tau = 500$ μs, 1024 transients coadded) on the porcine tendon sample in both orientations are given in Table 2. Gaussian broadening (300 Hz) was applied to the data and the full width of the powder pattern spectrum was 8 kHz. For each orientation, the relaxation rate was measured for different points of

TABLE 2
Double-Quantum Relaxation Rates, $R^{(2)}$, Measured in Porcine Achilles Tendon Using ^{23}Na NMR

Perpendicular to B_0 field		Parallel to B_0 field	
$R^{(2)}/s^{-1}$	F	$R^{(2)}/s^{-1}$	F
2640[a]	0.051	2760	0.11
2640	0.042	2560	0.099
2590	0.036	2380	0.087
2500	0.032	2170	0.087
2400	0.029	2000	0.080
2270	0.028	1850	0.066
2140	0.027	1730	0.067
1990	0.027	1720	0.070
1850	0.027	1790	0.066
1740	0.029	1920	0.076
1650[b]	0.037	—	—

[a] Rate measured near outside edge of ^{23}Na satellite lineshape.
[b] Rate measured near middle of ^{23}Na satellite lineshape.

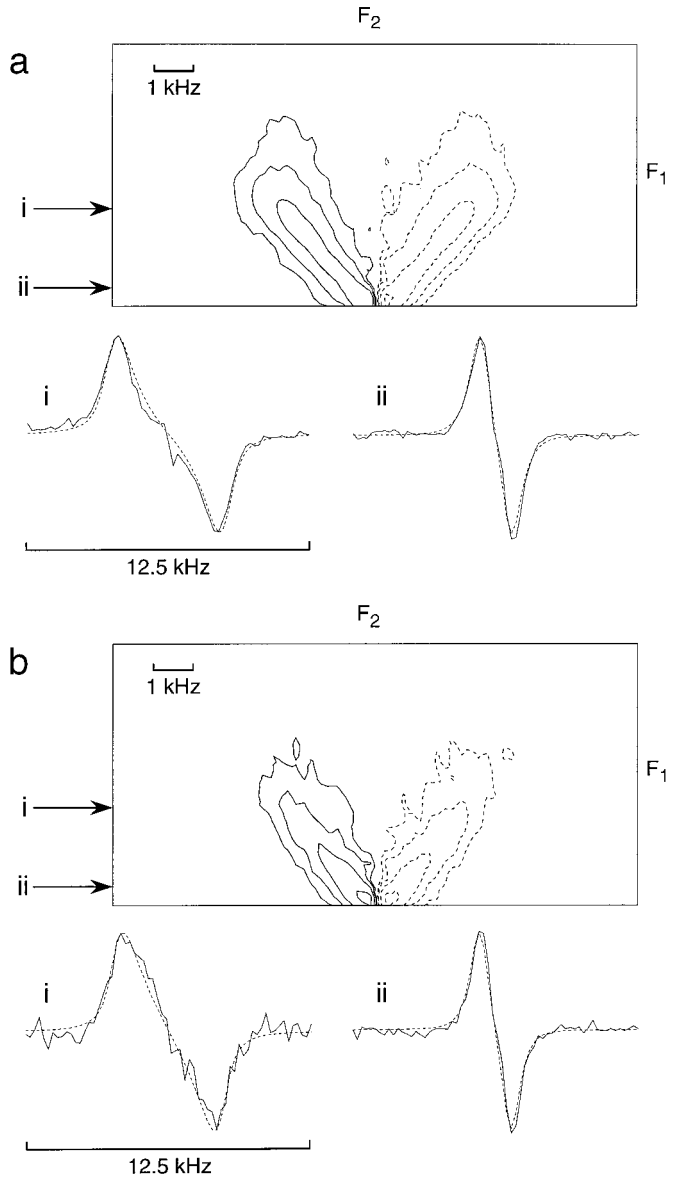

FIG. 2. Two-dimensional Jeener–Broekaert ^{23}Na NMR spectra of porcine Achilles tendon oriented perpendicular to B_0 in (a) and parallel to B_0 in (b). Thirty-two increments in t_1, each with 1024 transients coadded, 180° pulse length 70 μs. Cross sections (i and ii, solid lines) extracted from each two-dimensional spectrum have been fitted with analytical lineshape expressions (dashed lines).

the powder pattern by extracting columns from the two-dimensional data set $S(\Delta, \omega_2)$. The first rate shown in each case comes from the outside of the powder pattern and subsequent values correspond to points moving inward toward the central transition. The interesting feature of these relaxation rates is the apparent decrease across the powder pattern. This decrease occurs for both orientations and is indicative of anisotropy in the relaxation, that is, a dependence of the relaxation rate on the orientation of the local director or, in other words, a dependence of $J_n(\omega)$ on the value of θ. Such anisotropy is not unexpected but has not been observed in this type of system previously. Note that, since $R^{(2)} = R_1^{(1)}$, we have effectively detected anisotropy in the transverse relaxation rate. A similar procedure applied to the Jeener–Broekaert experiment measuring quadrupolar order relaxation failed to show any anisotropy. This implies, by inspection of Eq. [1], that the anisotropy arises from the $J_0(0)$ (zero frequency) component of the relaxation function. In turn, this implies that slow motions are responsible for the anisotropic relaxation, suggesting the likelihood that either Model C or E will provide the best theoretical description of the motion of the ions in this sample. Note that no anisotropy in the relaxation was observed in the bovine nasal cartilage sample.

Extraction of Linewidths from Two-Dimensional Jeener–Broekaert Spectra

Two-dimensional Jeener–Broekaert spectra were obtained from the porcine Achilles tendon sample described above. Figure 2 shows the spectra obtained with the sample oriented perpendicular to the static magnetic field (Fig. 2a) and parallel to the field (Fig. 2b). It can be immediately seen that the two spectra have different lineshapes. The change of lineshape due to the orientation with respect to the B_0 field can be attributed to macroscopic ordering of collagen fibers in the tendon. Several cross sections were taken through each of the two-dimensional spectra and fitted to an analytical function based on a quadratic distribution function. Two cross sections from each spectrum, corresponding to the arrows marked, and the fitted functions are shown. The relaxation rates determined are given in Table 3 for all cross sections that gave a reliable fit.

Two features can be noted from these results. First, the

TABLE 3

Extraction of Satellite Transition Relaxation Rates, $R_1^{(1)}$, from Two-Dimensional Jeener–Broekaert ^{23}Na NMR Spectra of Porcine Achilles Tendon

Perpendicular to B_0 field		Parallel to B_0 field	
$R_1^{(1)}/s^{-1}$	F	$R_1^{(1)}/s^{-1}$	F
2870[a]	0.064	—	—
2760	0.071	—	—
2610	0.069	2550	0.10
2480	0.045	2560	0.090
2320	0.065	2270	0.10
2270	0.070	2390	0.10
2140	0.037	2350	0.063
1910	0.055	1830	0.057
1950	0.043	2100	0.055
2360	0.059	2410	0.067
2100	0.033	1880	0.045
1850[b]	0.048	1660	0.058

[a] Rate measured near outside edge of ^{23}Na satellite lineshape.
[b] Rate measured near middle of ^{23}Na satellite lineshape.

TABLE 4
Mean-Square Residuals after Simultaneous Fitting of Theoretical Models to Jeener–Broekaert ^{23}Na NMR Spectra Obtained from Samples 1–7 (See Text)

	Model				
Sample	A	B	C	D	E
1	**0.299 ± 0.003**	0.310 ± 0.002	0.358 ± 0.004	0.42 ± 0.06	0.36 ± 0.01
2	**0.39 ± 0.08**	0.39 ± 0.08	0.41 ± 0.08	0.40 ± 0.08	0.47 ± 0.1
3	0.80 ± 0.01	0.36 ± 0.01	0.169 ± 0.008	0.23 ± 0.02	**0.15 ± 0.01**
4	0.70 ± 0.01	0.282 ± 0.008	0.256 ± 0.008	**0.08 ± 0.01**	0.09 ± 0.01
5	1.06 ± 0.08	0.835 ± 0.06	0.26 ± 0.04	0.46 ± 0.05	**0.17 ± 0.04**
6	0.69 ± 0.06	0.42 ± 0.06	0.27 ± 0.06	**0.24 ± 0.06**	0.24 ± 0.06
7	1.0 ± 0.2	0.8 ± 0.1	0.5 ± 0.1	0.4 ± 0.1	**0.2 ± 0.1**

Note. Best fits are shown in bold.

values for the relaxation rate $R_1^{(1)}$ are of the same order as the values for $R^{(2)}$ obtained from the DQQE experiment, confirming both approaches to the measurement of the relaxation rate. Second, the variation of the relaxation rate with quadrupolar splitting confirms the observation of anisotropy in the relaxation made by measurement of the double-quantum relaxation rate. The reduction in the relaxation rate can also be seen by inspection of the cross sections in Fig. 2, which clearly show a decrease in linewidth for the cross sections taken nearer to zero frequency in F_1.

Lineshape Fitting

Lineshapes simulated in accordance with the analytical function in Eq. [13] and Models A to E were fitted to sets of ^{23}Na NMR spectra recorded by application of the Jeener–Broekaert pulse sequence shown in Fig. 1a to a number of model biological systems. Each set consisted of spectra observed with different evolution times, τ, but with all other parameters equal.

For each of the seven samples described below, sets of one-dimensional NMR Jeener–Broekaert spectra with an incremented τ period were acquired. Except where noted, all spectra were recorded at 105.8 MHz on a Bruker MSL 400 spectrometer with a 180° pulse length of 16 μs and 2048 transients per creation-time increment. A simultaneous fit to 10 spectra with different τ periods was performed several times with different starting points for each sample and model. The final "residuals" are the average of the mean-square differences obtained from the fits while the error ranges reflect the standard error in the results and the spectral resolution. Table 4 shows the values of the residuals obtained by fitting each sample with all five theoretical models. The model resulting in the lowest residual is considered the most appropriate for that sample, with the caveat that if the residuals for two models differ by less than the error range, the simpler model is deemed more appropriate. Table 5 gives the parameters obtained from the best of the fits in Table 4.

Sample 1 is a lamellar-phase, lyotropic liquid–crystal sample consisting of a 1:2:2 mixture of sodium octanoate, 1-decanol, and water, and prepared in accordance with Sasanuma *et al.* (*26*). Such a system contains well-ordered organic bilayers to which sodium ions are associated and is generally thought to contain only one ^{23}Na environment which is oriented randomly with respect to B_0. This is an approximation to the binding of biological sodium ions to cell membranes. Table 4 shows that the spectra from Sample 1 are best approximated by Model A, indicative of a homogeneous sample containing only one environment for ordered ions. Figure 3a demonstrates the overlaying of experimental and simulated lineshapes for three typical spectra from the set fitted. The features of the antiphase

TABLE 5
Lineshape and Motional Parameters Corresponding to Best Fits in Table 4

	⟨Sample⟩		
Model A	1	2	
$\omega_Q^{max}/(2\pi$ Hz)	2764 ± 4	1446 ± 2	
$K/(\omega_0$ s$^{-1})$	17 ± 3	160 ± 40	
$\omega_0\tau_c$	0.14 ± 0.02	0.6 ± 0.1	
Model D	4	6	
$\langle\omega_Q^{max}\rangle/(2\pi$ Hz)	520 ± 10	1720 ± 10	
$\Delta\omega_Q^{max}/(2\pi$ Hz)	410 ± 20	760 ± 20	
$K\{J_0(0) + J_1(\omega_0)\}$/s^{-1}	112 ± 7	330 ± 10	
$KJ_2(2\omega_0)$/s^{-1}	120 ± 7	345 ± 5	
Model E	3	5	7
$\langle\omega_Q^{max}\rangle/(2\pi$ Hz)	210 ± 10	1500 ± 200	1380 ± 20
$\Delta\omega_Q^{max}/(2\pi$ Hz)	210 ± 30	2900 ± 300	1520 ± 30
KJ^f/s^{-1}	3.7 ± 0.3	65 ± 4	70 ± 10
$KJ_0^s(0)$/s^{-1}	2500 ± 40	13000 ± 1000	2500 ± 100
$KJ_2^s(0)$/s^{-1}	7 ± 3	200 ± 60	500 ± 200

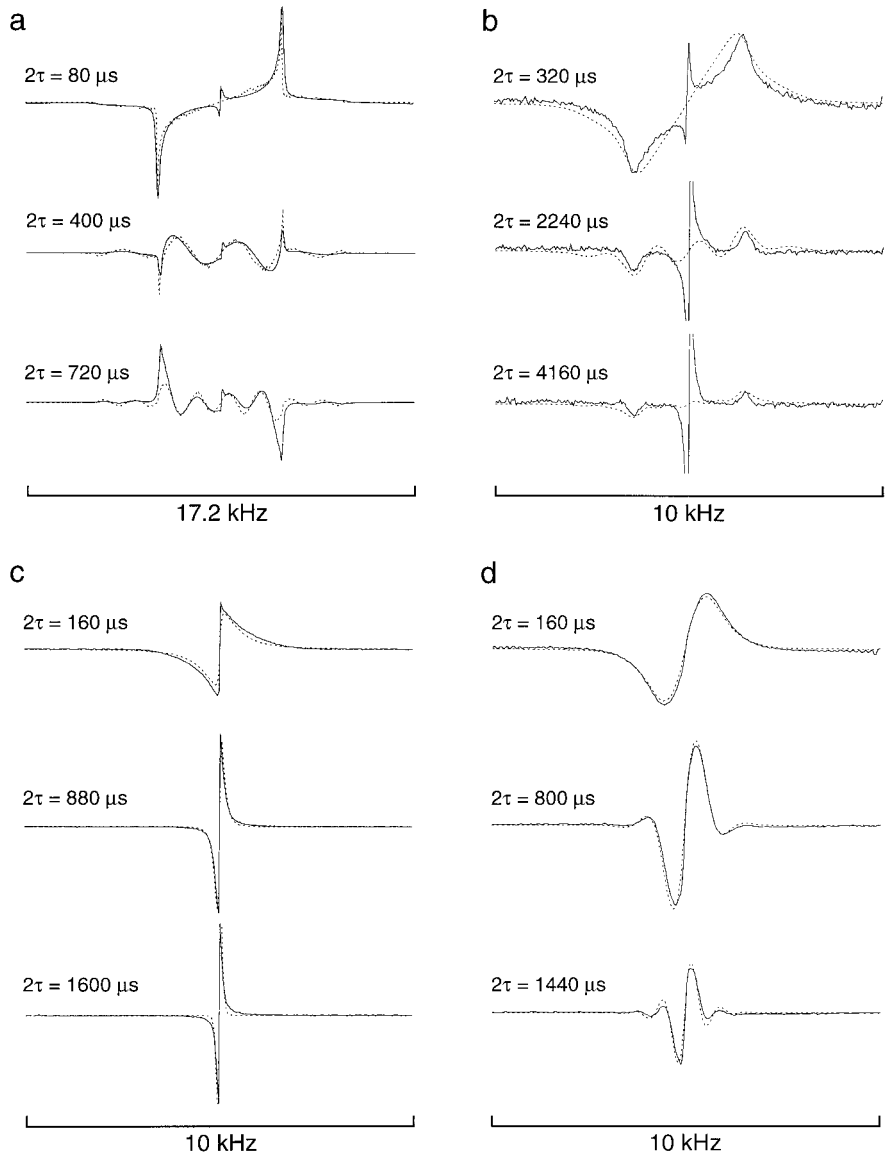

FIG. 3. Jeener–Broekaert ^{23}Na NMR spectra obtained from Samples 1–4 using three values of the evolution time, 2τ, (solid lines) and results of simultaneous lineshape fitting (dashed lines). (a) Sample 1, lyotropic liquid crystal. Best fit: Model A. (b) Sample 2, egg phosphatidylcholine in 0.15 M NaCl. Best fit: Model A. (c) Sample 3, collagen in 0.15 M NaCl. Best fit: Model E. (d) Sample 5, bovine articular cartilage. Best fit: Model D.

Pake powder patterns can be clearly seen, as can the periodic nodes resulting from the (approximately) sinusoidal dependence of the lineshape on the value of $4\omega_Q\tau$ (Eq. [13]). The parameter $K\tau_c$ is related to the linewidth due to relaxation (i.e., the homogeneous linewidth). In this sample this parameter is much smaller than the value of ω_Q^{max} as would be expected for a true solid.

Sample 2 is a sample of multilamellar vesicles prepared by suspending L-α-phosphatidylcholine (type X) from dried egg yolk (Sigma) in 0.15 M NaCl. This sample is also best described by Model A, with a single ^{23}Na environment but, in contrast to Sample 1, the homogeneous and heterogeneous linewidths are more comparable. The sample is thus a much better approximation to biological membranes and it yields spectra of a quite different appearance. Figure 3b shows three typical fitted spectra from the data set. All of the experimental spectra are corrupted by a central artifact due to incomplete suppression of the signal from ions in the extreme-narrowing limit which, in this sample, vastly outnumber the ordered ions. These data points were discarded during the fitting procedure.

Sample 3 is a sample of collagen (type I) obtained from bovine Achilles tendon (Sigma) in 0.15 M NaCl. The spectra obtained from this sample show particularly interesting behavior as a function of 2τ. Instead of developing the expected nodes as 2τ increases, the lineshape simply narrows (Fig. 3c).

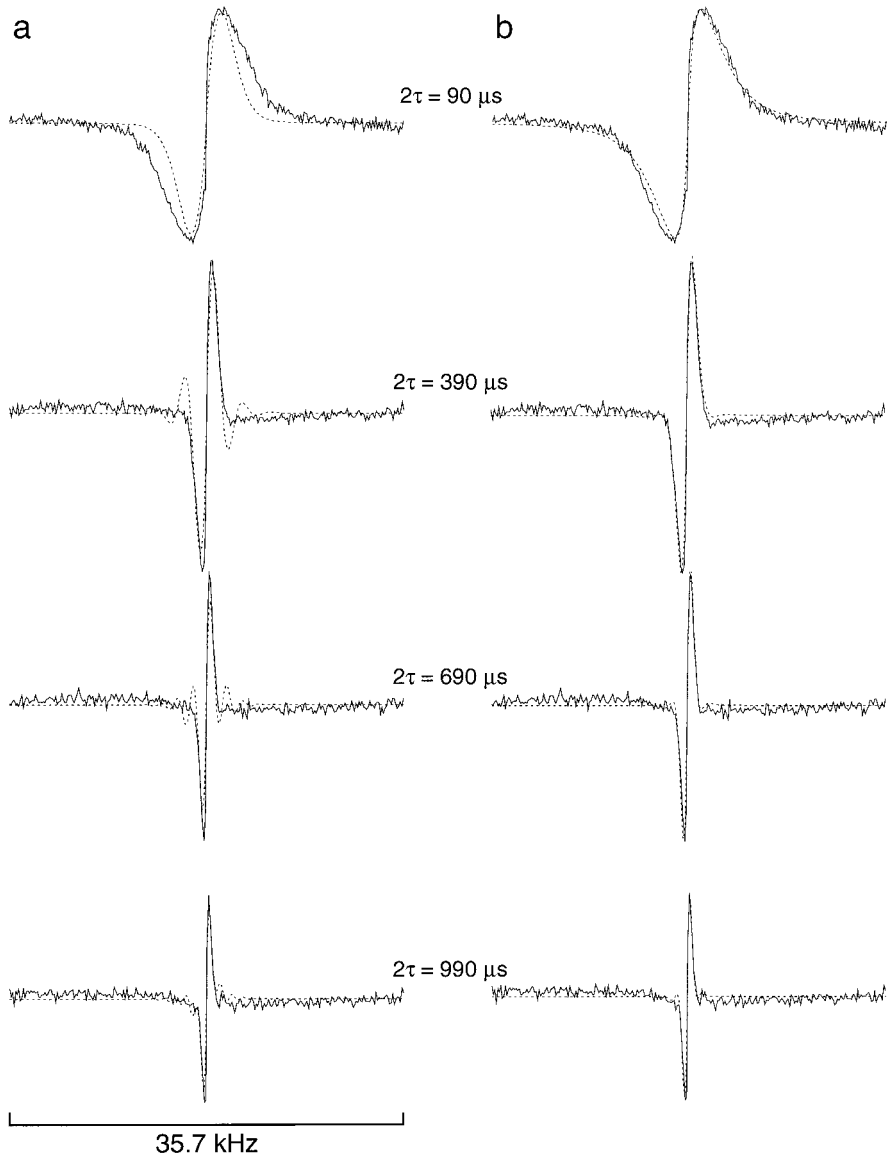

FIG. 4. Four typical Jeener–Broekaert ^{23}Na NMR spectra (solid lines) of Sample 5, bovine tendon, showing the results of fits (dashed lines) using (a) Model D and (b) Model E.

The spectra are best fitted by Model E in which the spectral densities possess a θ-dependence due to anisotropic local motion in the presence of the macromolecular fibers. A very large value of $KJ_0^s(0)$ relative to the other spectral density components (KJ^f and $KJ_2^s(0)$) is required in order to model the behavior of the experimental spectra. Note that the homogeneous linewidth, dominated by the $KJ_0^s(0)$ term, is much larger than the value of $\langle\omega_Q^{max}\rangle$, providing an explanation for the absence of nodes in the spectra. The model also requires a large range of ω_Q^{max} values (i.e., a large value of $\Delta\omega_Q^{max}$ relative to $\langle\omega_Q^{max}\rangle$), indicating a high degree of heterogeneity in the ionic environment.

Sample 4 is an excised tissue sample of bovine articular cartilage, stored in 0.15 M NaCl. The presence of collagen has been demonstrated to be the origin of ordered ions in this sample (*4*). However, unlike in the case of collagen, spectra obtained from this sample display the nodes (Fig. 3d). The experimental data are fitted well by Model E, but better by the simpler Model D, which has no θ-dependence in the spectral densities.

Sample 5 is an excised tissue sample of bovine tendon from around the knee, stored in 0.15 M NaCl to maintain cell structure. Bovine tendon is known to contain collagen molecules which might order ^{23}Na nuclei in a similar way to those in Sample 3. Figure 4 compares fits using Models D and E for several spectra from this sample. These spectra are

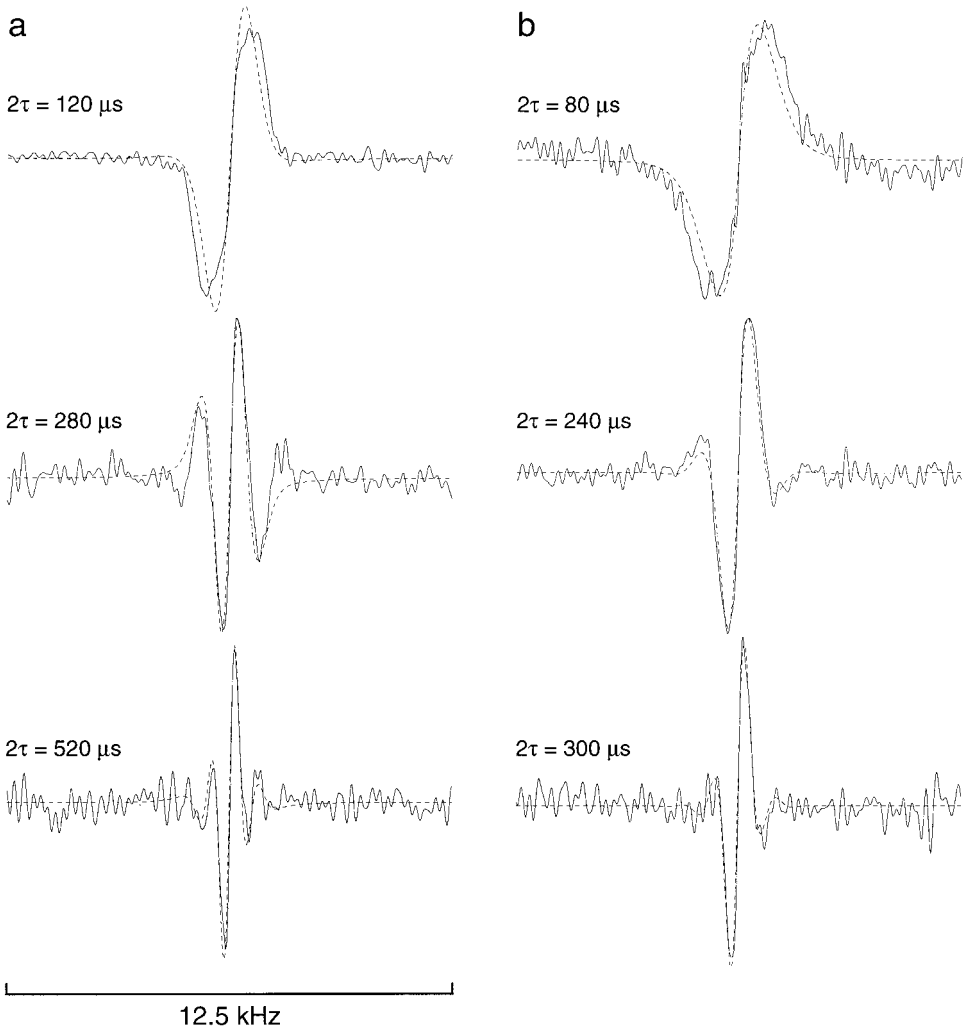

FIG. 5. Jeener–Broekaert ^{23}Na NMR spectra (solid lines) of porcine Achilles tendon oriented perpendicular to B_0 in (a) and parallel to B_0 in (b), obtained with three different values of the evolution time, 2τ, and results of simultaneous lineshape fitting (dashed lines). Best fit: (a) Model D; (b) Model E.

best fitted by Model E and their appearance is remarkably similar to those from Sample 3, suggesting a similar ordering of ^{23}Na nuclei by collagen. As with the collagen sample, the absence of nodes can only be accounted for by Model E which includes a mechanism that allows the homogeneous linewidth to dominate the quadrupolar splitting.

Samples 6 and 7 consist of porcine tendon aligned perpendicular or parallel to B_0, respectively. Tendon is an inherently anisotropic sample on the macroscopic level. Figure 2 demonstrates the dependence of two-dimensional Jeener–Broekaert spectra on the orientation of the tendon with respect to the static magnetic field. Simultaneous fits can be performed using the same data sets (recorded on the Biospec at 79.5 MHz) but only performing a Fourier transform in the t_2 dimension. Sample 6 is fitted well by both models so the simpler Model D is preferred, while Sample 7 is fitted better by Model E. The resulting parameters are given in Table 5 and typical fits are shown in Fig. 5. Model E implies anisotropic local motions resulting in an orientational dependence of $J_0(0)$ and hence anisotropic relaxation. Clearly, the motion will not change depending on the orientation of the sample. The difference in the fits can be ascribed to the macroscopic ordering of the collagen fibers in the tendon. From Eq. [17b] it can be seen that, for Model E, the contribution of the $J_0^s(0)$ term to $J_0(0)$ is greater by a factor of four when $\theta = 0°$ than when $\theta = 90°$. Thus, when the majority of fibers are aligned with B_0, as in Sample 7, the θ-dependence of $J_0(0)$ will be more evident and Model E is more likely to give an improvement in the fit. However, in Sample 6, the fibers are perpendicular to B_0, the θ-dependence of $J_0(0)$ will be less evident, and the fitting procedure will be less likely to distinguish between the two models. It is therefore reasonable to conclude that Model E provides the best model of the environment in the porcine tendon sample.

CONCLUSIONS

Three methods of analysis to be used to extract quantitative information from spectra of ordered sodium in biological systems have been demonstrated. Measurements of quadrupolar order relaxation have provided evidence of compartmentation in bovine nasal cartilage, while the relaxation of double-quantum coherence determined by a DQQE experiment indicates anisotropy in the relaxation in porcine tendon. This anisotropy was confirmed by the determination of the homogeneous linewidth by fitting to cross sections through two-dimensional Jeener–Broekaert spectra.

Simultaneous fitting of detailed expressions for the lineshape to one-dimensional spectra provides further information about the local environment of the ordered sodium. A simple model, with unique values for ω_Q^{max} and the correlation time and exhibiting macroscopic disorder, has been shown to yield the best fits for samples containing ^{23}Na associated with membrane-like structures (Samples 1 and 2). This model is compatible with the assumption of the presence of a unique binding site for the ions which are in fast exchange with ions in free solution (*27*).

However, samples containing collagen (Samples 3 to 7) are fitted very badly by this model and are instead best described by either Models D or E, which both account for sample heterogeneity. Model E includes an orientational dependence in the expression for the spectral densities, based on lateral and radial diffusion motions around the collagen fibers. This is the most suitable description of the environment of sodium in the porcine tendon sample, confirming the observation of anisotropy in the relaxation made using the other two analysis methods and giving a more detailed description of the environment and motion of the sodium ions in the tendon.

The measurement of relaxation rates, extraction of homogeneous linewidths from cross sections through two-dimensional Jeener–Broekaert spectra, and simultaneous fitting to a series of one-dimensional Jeener–Broekaert spectra are all powerful complementary tools for the elucidation of ionic interactions with ordered structures. The analysis methods presented here can be applied to the study of any spin $I = \frac{3}{2}$ nucleus exhibiting order in biological systems and permit the detailed investigation of ordered environments.

ACKNOWLEDGMENTS

We acknowledge generous support by the Royal Society. R.K.-H. thanks the Medical Research Council for the award of a research studentship (1993–1996). We are grateful to Professors George Radda and Peter Styles for their interest and support and to Paul Hodgkinson for writing the software used to process the spectra presented here. The MSL 400 spectrometer was purchased with the aid of a grant from the Science and Engineering Research Council.

REFERENCES

1. U. Eliav, H. Shinar, and G. Navon, *J. Magn. Reson.* **98,** 223 (1992).
2. H. Shinar, T. Knubovets, U. Eliav, and G. Navon, *Biophys. J.* **64,** 1273 (1993).
3. R. Kemp-Harper and S. Wimperis, *J. Magn. Reson. B* **102,** 326 (1993).
4. U. Eliav and G. Navon, *J. Magn. Reson. B* **103,** 19 (1994).
5. J. S. Tauskela and E. A. Shoubridge, *Biochim. Biophys. Acta* **1158,** 155 (1993).
6. R. Kemp-Harper, S. P. Brown, P. Styles, and S. Wimperis, *J. Magn. Reson. B* **105,** 199 (1994).
7. J. S. Tauskela, J. M. Dizon, P. J. Cannon, and J. Katz, *J. Magn. Reson. B* **108,** 165 (1995).
8. R. Reddy, L. Bolinger, M. Shinnar, E. Noyszewski, and J. S. Leigh, *Magn. Reson. Med.* **33,** 134 (1995).
9. T. Knubovets, H. Shinar, U. Eliav, and G. Navon, *J. Magn. Reson. B* **110,** 16 (1996).
10. D. Liu, P. A. Knauf, and S. D. Kennedy, *Biophys. J.* **70,** 715 (1996).
11. D. Liu, S. D. Kennedy, and P. A. Knauf, *Biochemistry* **35,** 15228 (1996).
12. C. E. Hughes, R. Kemp-Harper, P. Styles, and S. Wimperis, *J. Magn. Reson. B* **111,** 189 (1996).
13. U. Eliav and G. Navon, *J. Magn. Reson. A* **115,** 241 (1995).
14. R. Kemp-Harper, S. P. Brown, C. E. Hughes, P. Styles, and S. Wimperis, *Prog. NMR Spectrosc.* **30,** 157 (1997).
15. C. E. Hughes, R. Kemp-Harper, and S. Wimperis, *J. Chem. Phys.* **108,** 876 (1998).
16. S. P. Brown and S. Wimperis, *J. Magn. Reson. B* **109,** 291 (1995).
17. G. Jaccard, S. Wimperis, and G. Bodenhausen, *J. Chem. Phys.* **85,** 6282 (1986).
18. J. Jeener and P. Broekaert, *Phys. Rev.* **157,** 232 (1967).
19. U. Eliav and G. Navon, *J. Magn. Reson.* **130,** 63 (1998).
20. D. E. Woessner and N. Bansal, *J. Magn. Reson.* **133,** 21 (1998).
21. S. Wimperis, *in* "Encyclopedia of Nuclear Magnetic Resonance" (D. M. Grant and R. K. Harris, Eds.), Vol. 6, p. 4078, Wiley, Chichester (1996).
22. S. P. Brown and S. Wimperis, *Chem. Phys. Lett.* **224,** 508 (1994).
23. T. R. J. Dinesen and B. C. Sanctuary, *J. Chem. Phys.* **101,** 7372 (1994).
24. A. Abragam, "Principles of Nuclear Magnetism," p. 447, Oxford Science Publications, Oxford (1961).
25. B. Halle, *Mol. Phys.* **60,** 319 (1987).
26. Y. Sasanuma, M. Nakamura, and A. Abe, *J. Phys. Chem.* **97,** 5155 (1993).
27. W. D. Rooney and C. S. Springer, Jr., *NMR Biomed.* **4,** 209 (1991).